Pulse shaping in the mid-infrared by a deformable mirror

Andrea Cartella,[1,*] Stefano Bonora,[2] Michael Först,[1] Giulio Cerullo,[3] Andrea Cavalleri,[1,4] and Cristian Manzoni[3]

[1]*Max-Planck Institute for the Structure and Dynamics of Matter, Hamburg, Germany*

[2]*IFN-CNR, LUXOR, Padova, Italy*

[3]*IFN-CNR, Dipartimento di Fisica—Politecnico di Milano, Milan, Italy*

[4]*Department of Physics, Clarendon Laboratory, University of Oxford, Oxford, UK*

**Corresponding author: andrea.cartella@mpsd.mpg.de*

Received December 20, 2013; revised February 6, 2014; accepted February 6, 2014; posted February 10, 2014 (Doc. ID 203526); published March 11, 2014

Femtosecond pulses at mid-infrared (MIR) wavelengths can be used to drive low energy excitations in molecules and solids [1] and have been shown to control insulator-metal transitions [2] or magnetism [3] and superconductivity [4]. Furthermore, shaped MIR pulses can be applied to small molecule photochemistry and used for vibrational ladder climbing [5,6].

Temporal shaping of ultrashort laser pulses requires control of the phase and amplitude of their electric field in the frequency domain. This is typically achieved using a $4f$ zero dispersion pulse shaper, which allows to directly manipulate the individual frequency components in the Fourier plane. Using this approach, many different pulse-shaping techniques have been developed in the past, based on liquid crystal spatial light modulators (LC-SLMs) or acousto-optic modulators (AOMs), leading to the successful control of the pulse shape in the visible and near-infrared spectral regions [7].

Since the MIR light pulses are usually generated by difference frequency generation (DFG) between two near-infrared beams, one additional and straightforward approach to shaping MIR pulses consists in applying pulse shapers to one of the near-infrared beams and subsequently transferring the phase modulation through the DFG process [8–11]. The drawbacks of this indirect pulse-shaping technique are the nonlinearity of the DFG process, affecting the fidelity of phase control, and the fact that the shaping considerably reduces the peak intensity of the near-infrared pulses, making the efficiency of the DFG process strongly dependent on the specific pulse shape. The approach based on direct manipulation of the MIR pulse is generally more challenging, since it calls for the development of phase modulators capable of handling long wavelengths. A first example was shown by Kaindl *et al.* [12], where shaping the spectral amplitude of pulses at 12.5 μm was achieved by placing patterned masks at the Fourier plane of a $4f$ pulse shaper. More complex phase and amplitude manipulation is not straightforward with LC-SLMs because they do not transmit wavelengths longer than 1.6 μm. Complex pulse shaping is instead possible with Germanium (Ge)-based AOMs, although Ge begins to absorb at 12 μm [13]. Recently, amplitude and phase shaping was extended to 20 μm by a calomel-based acousto-optic programmable dispersive filter [14].

Deformable mirrors (DMs) placed in the Fourier plane of a $4f$ pulse shaper can introduce smooth phase variations by the deformation of a thin membrane or of a semi-passive bimorph structure [15–17]. DMs can be used for phase-only modulation, with the important advantages of high throughput and being substantially achromatic. This allows the extension of the spectral coverage to the MIR, limited only by the reflectivity of the metallic coating. Pulse shaping typically requires the application of spectral phase shifts, ϕ, as high as 5–10 optical cycles. In DM-based pulse shapers a phase shift at a component, λ, requires a mirror deformation, $\Delta z = \lambda \cdot \phi/4\pi$. In the 10–20 μm wavelength region this deformation may be very large and cannot be achieved with standard membrane mirrors. Therefore, a new DM has to be designed, realized, and characterized.

In this Letter, we present a DM-based pulse shaper specially designed to operate at MIR wavelengths from 10 to 20 μm (15–30 THz). This device is built in a grating-based $4f$ geometry, with a large-stroke DM in its Fourier plane. We prove the ability to compress femtosecond MIR pulses, to impart quadratic and cubic spectral phases, and to split the input beam spectrum generating two independent pulses.

The scheme of the pulse shaper is sketched in Figs. 1(a) and 1(b). The different spectral components of the beam are spatially dispersed by a diffraction grating (40 lines/mm, blazed at 15 μm) and collected by a gold spherical mirror with $f = 50$ cm. Each wavelength, λ, is then mapped on one coordinate of the DM, reflected back slightly lower than the incoming direction, and picked up by a flat mirror. The shaper focal length and the geometrical arrangement, with the DM on top of the grating, were carefully chosen to minimize chromatic aberrations in the focus of the shaped beam.

Our DM is a unique piezoelectric push–pull structure. It consists of a rectangular (10 mm × 90 mm) gold coated silicon substrate that can be bent by a series of 32 piezoelectric actuators [Fig. 2(a)]. Applying a voltage to one actuator locally distorts the mirror surface, as sketched in Fig. 2(b). Both convex and concave curvatures can be

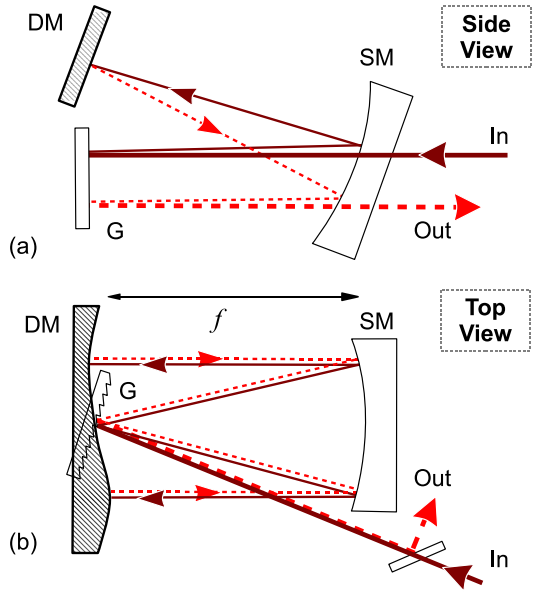

Fig. 1. Side (a) and top (b) view of the pulse shaper: DM, deformable mirror; SM, spherical mirror; G, grating.

achieved, according to the voltage polarity. When more than one actuator is powered, the resulting shape of the mirror surface is the linear superposition of the deformations produced by each of them, therefore without cross talk effects. Typical DMs developed for the visible and ultraviolet spectral range exhibit deformations on the order of a few micrometers. In order to achieve the large deformations required here, the DM has a larger reflecting area and a thinner, more elastic substrate, with a surface flatness compatible with the long working wavelengths. Due to the large stroke, the characterization of the mirror response to the applied voltages could not be performed with standard techniques (optical interferometry and wavefront sensing). Instead, the DM influence functions have been characterized by measuring a Moiré pattern resulting from the application of a 150 V voltage to each single electrode. Figure 2(c) shows an example of a Moiré pattern (lower panel), together with the deformations of some electrodes. The blue line shows the combined action (scaled by a factor of 10) of all the actuators, resulting in deformations as large as ±110 μm. Figure 2(d) shows the detailed deformation deduced from SEA-TADPOLE measurements [18] when both positive and negative voltages are applied to one of the central actuators. The phase modulation achievable with this DM is continuous and smooth. The desired deformation can be easily controlled by software and applied in less than one second. The driving electronics has an 8-bit resolution, meaning that the actuators can be moved in 256 steps from one end to the other. When all the actuators are powered, the center of the mirror can move by 220 μm (±110 μm from the flat position). Consequently, the minimum surface deformation applicable is about one micrometer. This limits the employment of the DM to wavelengths larger than 10 μm. In the spectral range between 10 and 20 μm, the reflectivity of the DM is about 95%. The overall throughput of the shaper, including the other mirrors and the grating, is close to 50%.

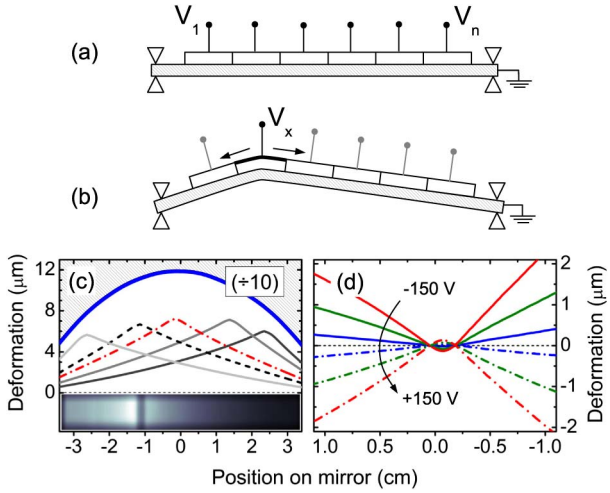

Fig. 2. Structure and characterization of the DM. (a), (b) Lateral section of the mirror structure, showing the sequence of piezoelectric actuators and their effect when a voltage is applied. (c) Influence functions of some actuators deduced by Moiré interferometry after application of a 150 V voltage. The lower panel displays the measured Moiré pattern corresponding to the dashed line. The blue curve is the deformation of the mirror (scaled by a factor of 10) when voltages of 150 V are applied to all electrodes. (d) Mirror shape after the application of different voltages to one of the actuators [dash-dotted line of panel (c)], characterized by SEA-TADPOLE measurements.

We demonstrate the capabilities of this shaper using few-cycle MIR pulses, obtained by DFG between two near-infrared pulses from optical parametric amplifiers (OPAs) at 1 kHz repetition rate. The system can generate MIR pulses tunable up to 20 μm (i.e., down to 15 THz) [19]. Since the OPAs are seeded by the same white light continuum (WLC), the MIR pulses are carrier envelope phase stable [20,21]. Thus, their electric field can be easily measured by electro-optical sampling (EOS), using 30 fs pulses from the Ti:sapphire amplifier feeding the OPAs. This approach gives direct access to the electric field profile of the MIR pulses and to their spectral phase via Fourier and Wigner transformations.

Figure 3(a) displays a Wigner distribution map of a typical 19 THz MIR pulse after passing through the shaper. With a flat DM this pulse is nominally unaffected by the shaper. We obtain a spectral bandwidth of 2 THz (FWHM) and a pulse duration of 417 fs. In order to compress the pulse, we retrieve the spectral phase from this

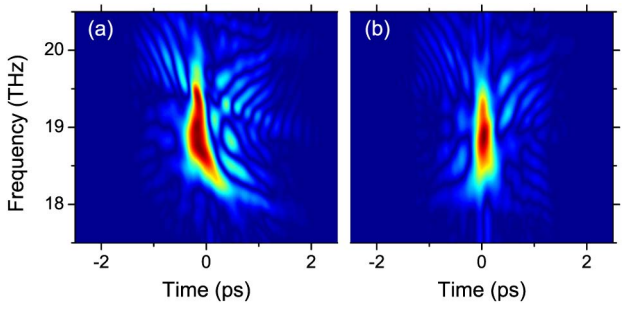

Fig. 3. Wigner maps of (a) a typical MIR pulse measured with the DM set to flat, i.e., unaffected by the shaper and (b) after a single iteration of phase compensation.

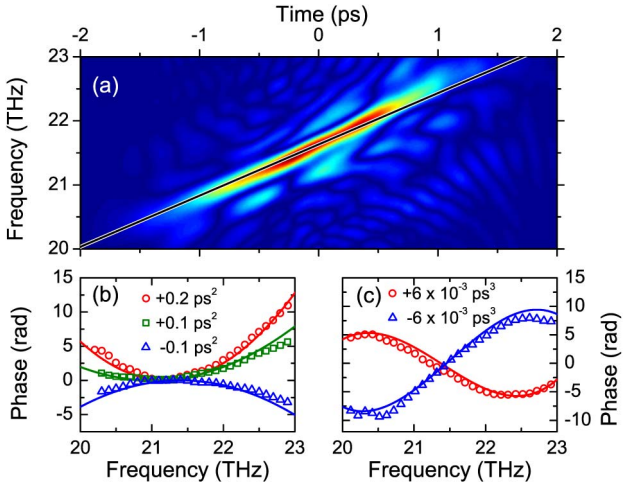

Fig. 4. (a) Wigner map of a measured pulse where a quadratic spectral phase with GDD = +0.2 ps^2 was applied. (b) Measured spectral phases of pulses with +0.2 ps^2 (red circles), +0.1 ps^2 (green squares) and –0.1 ps^2 (blue triangles) GDDs. (c) Characterization of $+6\times10^{-3}$ ps^3 (red circles) and -6×10^{-3} ps^3 (blue triangles) TODs. The solid lines represent the target spectral phases.

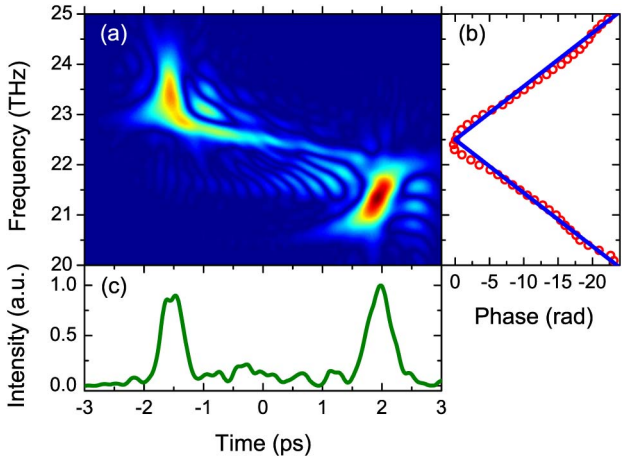

Fig. 5. (a) Wigner map of a double pulse. (b) Measured (red circles) compared with target (solid blue) spectral phase. (c) Temporal profile of the double pulse.

measurement and calculate the mirror deformation necessary to compensate for it. This deformation then defines the required electrode voltages through the DM influence functions. The result of a single iteration of this procedure is shown in Fig. 3(b), where the pulse duration has been reduced to 389 fs.

In the following, we characterize the shaper output in response to various spectral phase profiles. We first introduced a parabolic phase corresponding to a group delay dispersion (GDD) of +0.2 ps^2 and, therefore, to a linear group delay. Figure 4(a) shows the Wigner map deduced from the EOS of the shaped pulse. The solid line represents the target group delay, in very good agreement with the measurement. The capability of applying both positive and negative GDDs is demonstrated in Fig. 4(b), where the measured spectral phases (open symbols) corresponding to nominally applied dispersion values of +0.1 ps^2 and –0.1 ps^2 (solid lines) are also shown. The mirror can also apply a pure third-order dispersion (TOD), as shown in Fig. 4(c), where we applied TOD values of $\pm6\times10^{-3}$ ps^3. Again, the solid lines represent the target spectral phases, demonstrating the excellent capability of this shaper to introduce specified spectral phases in a single iteration.

Finally, we used the shaper to split the input field into two subpulses with different spectral content. This was obtained by applying a V-shaped spectral phase, i.e., different linear phases, to two portions of the pulse spectrum. This results in two different group delays and, therefore, in the generation of two subpulses containing different frequencies. The time delay between the pulses can be tuned by varying the slopes of the two arms, whereas the splitting frequency depends on the position of the actuated electrode. The Wigner map of a double pulse obtained in this way is shown in Fig. 5(a). The measured spectral phase is shown in panel (b), matching the target very well. The temporal spacing between the two pulses associated with the given slope is expected to be 3.5 ps. The measured delay, reported in panel (c) where we display the intensity profile of the two pulses, shows a very good agreement with the target value.

In conclusion, we present a DM-based MIR pulse shaper designed to operate in the wavelength region between 10 and 20 μm, where material absorption prevents the applicability of well established techniques. The MIR spectral phase was controlled by a specially designed DM, in a reflective-only, grating-based, 4*f* configuration. We demonstrate its capability of compressing MIR pulses and imparting both quadratic and third-order spectral phases on demand. The shaper capability of splitting the input pulses into double pulses with arbitrary delay and splitting frequency is also demonstrated. These tailored pulses will be employed in experiments aimed at the coherent control of phase transitions in condensed matter.

The research leading to these results has received funding JRA-INREX from LASERLAB-EUROPE (grant agreement no. 284464, ECS Seventh Framework Programme).

References

1. M. Först, C. Manzoni, S. Kaiser, Y. Tomioka, Y. Tokura, R. Merlin, and A. Cavalleri, Nat. Phys. **7**, 854 (2011).
2. M. Rini, R. Tobey, N. Dean, J. Itatani, Y. Tomioka, Y. Tokura, R. W. Schoenlein, and A. Cavalleri, Nature **449**, 72 (2007).
3. M. Först, R. I. Tobey, S. Wall, H. Bromberger, V. Khanna, A. L. Cavalieri, Y.-D. Chuang, W. S. Lee, R. Moore, W. F. Schlotter, J. J. Turner, O. Krupin, M. Trigo, H. Zheng, J. F. Mitchell, S. S. Dhesi, J. P. Hill, and A. Cavalleri, Phys. Rev. B **84**, 241104 (2011).
4. D. Fausti, R. I. Tobey, N. Dean, S. Kaiser, A. Dienst, M. C. Hoffmann, S. Pyon, T. Takayama, H. Takagi, and A. Cavalleri, Science **331**, 189 (2011).
5. C. Ventalon, J. M. Fraser, M. H. Vos, A. Alexandrou, J.-L. Martin, and M. Joffre, Proc. Natl. Acad. Sci. USA **101**, 13216 (2004).
6. D. Strasfeld, S.-H. Shim, and M. Zanni, Phys. Rev. Lett. **99**, 038102 (2007).
7. A. Weiner, Rev. Sci. Instrum. **71**, 1929 (2000).
8. N. Belabas, J. P. Likforman, L. Canioni, B. Bousquet, and M. Joffre, Opt. Lett. **26**, 743 (2001).
9. T. Witte, K. Kompa, and M. Motzkus, Appl. Phys. B **76**, 467 (2003).

10. H.-S. Tan, E. Schreiber, and W. S. Warren, Opt. Lett. **27**, 439 (2002).
11. H.-S. Tan and W. Warren, Opt. Express **11**, 1021 (2003).
12. R. A. Kaindl, M. Wurm, K. Reimann, P. Hamm, A. M. Weiner, and M. Woerner, J. Opt. Soc. Am. **17**, 2086 (2000).
13. S.-H. Shim, D. B. Strasfeld, and M. T. Zanni, Opt. Express **14**, 13120 (2006).
14. R. Maksimenka, P. Nuernberger, K. F. Lee, A. Bonvalet, J. Milkiewicz, C. Barta, M. Klima, T. Oksenhendler, P. Tournois, D. Kaplan, and M. Joffre, Opt. Lett. **35**, 3565 (2010).
15. E. Zeek, K. Maginnis, S. Backus, U. Russek, M. Murnane, G. Mourou, H. Kapteyn, and G. Vdovin, Opt. Lett. **24**, 493 (1999).
16. J. Garduño-Mejía, A. H. Greenaway, and D. T. Reid, J. Opt. Soc. Am. B **21**, 833 (2004).
17. D. Brida, G. Cirmi, C. Manzoni, S. Bonora, P. Villoresi, S. De Silvestri, and G. Cerullo, Opt. Lett. **33**, 741 (2008).
18. P. Bowlan, P. Gabolde, A. Shreenath, K. McGresham, R. Trebino, and S. Akturk, Opt. Express **14**, 11892 (2006).
19. A. Sell, A. Leitenstorfer, and R. Huber, Opt. Lett. **33**, 2767 (2008).
20. G. Cerullo, A. Baltuška, O. Mücke, and C. Vozzi, Laser Photonics Rev. **5**, 323 (2011).
21. C. Manzoni, M. Först, H. Ehrke, and A. Cavalleri, Opt. Lett. **35**, 757 (2010).